 DOI: 10.1002/maco.200805198

Corrosion Concepts

In this forum readers will be able to present practical problems for discussion. It is envisaged that these contributions will include not only discussion of general problems and incidents of corrosion but that suggested remedies will also be presented and discussed. It is hoped that this exchange of knowledge and experience will become a permanent feature of this periodical. We are particularly anxious that both Senior Scientists and those with more practical experience will make use of this forum to exchange information, problems and potential remedies.

Pitting corrosion on 316L pipes in terephthalic acid (TA) dryer

Y. Gong, J. Cao, X.-H. Meng and Z.-G. Yang*

Grade 316L is a type of austenitic stainless steel with ultra-low carbon content and it exhibits superior corrosion resistance. However, pitting is always observed in 316L steel when it is exposed to media containing halide ions. In the present study, we found that in the presence of acetate acid (HAc) containing chloride or bromide ions, pitting occurred on the surface of the rotary steam pipes with the matrix material of 316L steel in terephthalic acid (TA) dryer. In order to identify the causes of the failure, metallographic structures and chemical compositions of the matrix material were inspected by an optical microscope (OM) and a photoelectric direct reading spectrometer. Beside these, scanning electron microscopy (SEM) and energy dispersive spectroscopy (EDS) as well as ion chromatography (IC) were used to analyze the micromorphologies of the corrosion pits and the chemical compositions of the corrosion deposits within them. Analysis of the results revealed the sources of halide ions and the factors accelerating the corrosion rate. Beside these, detailed mechanisms of pitting were discussed and six out of all the seven theoretical morphologies of pitting features were obtained in practice.

1 Introduction

Purified terephthalic acid (PTA) has wide applications in a variety of fields in our daily life, such as chemical fiber industry, light industry, electronics industry, and so on. Besides polyester bottle chips, polyester films, and polyester fibers, over 90% of the application of PTA is as the raw material to manufacture polyethylene terephthalate (PET) [1], one of the most widely used engineering plastics in the world. There are now two primary methods for manufacturing PTA, which are namely Witten process and Amoco process [2]. The Witten process was developed in the 50s of the 20th century, and thanks to its superior qualities such as simple and mature process, reliable technique, low corrosiveness, etc., it is still the most widely applied method currently available for manufacturing terephthalic acid (TA). However, the purity of the products produced by the Witten process is not ideal owing to the lack of purification procedures. The Amoco process is a relatively new method that can purify TA products immediately after obtaining the crude TA (CTA). Hence, the Amoco process has presently become more and more popular in many countries due to its simplified purification procedures [3].

The Amoco process has three major stages [4]:

- Manufacturing CTA

At this stage, the raw material *para*-xylene (PX) is oxidized in the atmosphere of oxygen or oxygen-rich air to produce TA, with cobalt acetate ($Co(Ac)_2$) and manganese acetate ($Mn(Ac)_2$) as catalysts, tetrabromoethane ($C_2H_2Br_4$) as the co-catalyst, and acetate acid (HAc) as the medium. Owing to its high content of impurities, particularly the byproducts, the

Y. Gong, J. Cao, X.-H. Meng, Z.-G. Yang
Department of Materials Science, Fudan University, No. 220 Handan Road, Shanghai 200433 (P. R. China)
E-mail: zgyang@fudan.edu.cn

TA product obtained during this stage is called CTA. Detailed reaction conditions and the chemical formula are shown in equation (1).

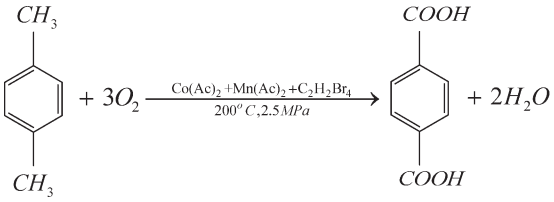

(1)

- Purifying CTA to PTA

The main byproduct of CTA produced in the oxidation stage is 4-carboxyl benzaldehyde (4-CBA). For the purpose of purification, 4-CBA is hydrogenated in hydrogen atmosphere to form soluble para-toluic acid (P-TA) in this stage, as seen in equation (2). By dissolving the P-TA in hot water, PTA is obtained. Meanwhile, the P-TA separated from CTA is also collected and recycled for further oxidation to produce PTA.

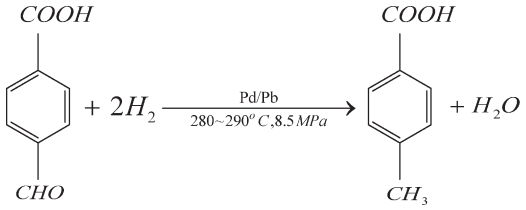

(2)

- Post-treatment of PTA

The so-called PTA obtained in the purification stage is far from the requirements of finished products. The wet PTA cakes must undergo some post-treatments at this stage, such as crystallization, drying, and packing for conversion into PTA powder.

In fact, there are several subsequent procedures also needed at stage 1 to get CTA, including centrifugation, filtering, and drying. Figure 1 presents the schematic view of the detailed procedures in stage 1 for manufacturing CTA in the industry. However, as is shown in equation (1), the complicated oxidation catalyst system may inevitably introduce a harmful environment involving bromide ions and HAc into the post-oxidation equipments such as TA centrifuge, vacuum filter, and a TA dryer. Furthermore, the alkali liquor (commonly 3% NaOH solution) applied to wash these equipments often contains some impurities, particularly chloride ions, which may cause even greater harm together with the existence of bromide ions and HAc. Therefore, various kinds of failures were frequently observed in TA centrifuge and TA dryer in the past during routine downtime.

316L stainless steel always suffers pitting corrosion in the presence of a medium containing halide ion [5, 6]. In this paper, we report various types of degradations such as pitting corrosion, crevice corrosion, flow-accelerated corrosion (FAC) and so on that were detected on some 316L steam pipe surfaces in the TA dryer of a CTA manufacturing device during an Amoco process in a petrochemical company in Shanghai. Among them, pitting corrosion was a major concern due to the serious harm it causes and its frequent occurrence on the pipes. The expected life of the TA dryer under the operating conditions was about 8 years, but some of its steam pipes failed due to pitting within just 2 years (from September 2004 to March 2007). Thus, detailed investigations from three aspects, matrix materials, process media, and service conditions were conducted on the pitting pipe, failure including macro and micromorphology observation on corrosion pits, and chemical composition analysis of the corrosion deposits in the pits. On the basis of the analysed results, the causes and the mechanisms of pitting are discussed, which have an important significance both for corrosion prevention of TA dryer in the future and also for a better understanding of pitting corrosion in engineering practice.

2 Experimental method and results

2.1 Visual observation

The TA dryer is a rotating cylinder with three arrays of circular steam pipes within the cylinder. In the dryer, steam passes

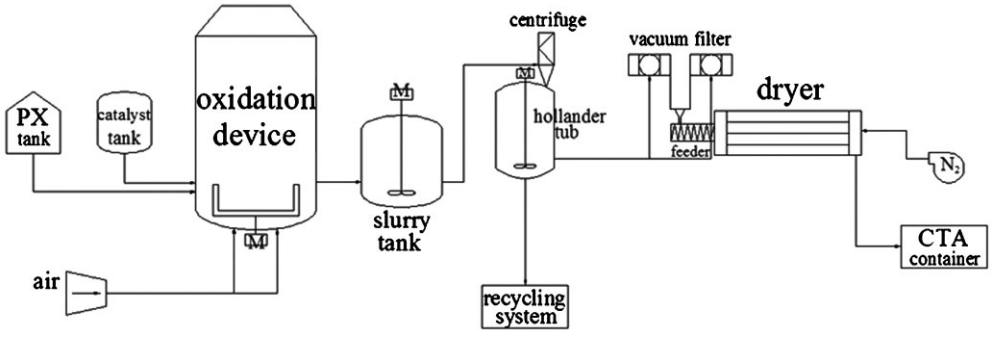

Figure 1. Schematic diagram of TA oxidation (CTA manufacturing) process

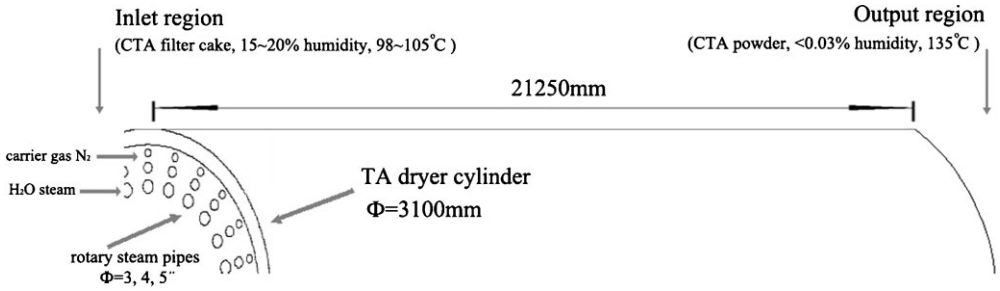

Figure 2. Schematic diagram of the operating conditions of TA dryer

through the steam pipes to heat the wet TA cakes that are transported outside the pipes from the inlet region of the dryer. Moreover, carrier gas (nitrogen) is sent in the opposite direction of the transportation of the cakes, i.e. from the output region of the dryer to remove the vapors evaporated from the cakes. More concrete details of the operating conditions of TA dryer can be referred from Fig. 2. In this paper, pitting dominantly took place at the inlet region of the steam pipes. Compared with the surface of the pitting-free pipes (Fig. 3(a)), which was smooth and plane, the surface of the pitted pipes was covered with a relatively large area of pits [Fig. 3(b)]. As shown in Fig. 3(c) and (d), many corrosion pits were randomly distributed on the pipe surface, and the depth of some pits even reached 0.5 mm.

2.2 Matrix material examination

Chemical compositions of the matrix materials in the inlet and output region of the steam pipes are listed in Table 1, which are in accordance with the requirements of SUS 316L specifications. The high content of Cr in 316L can facilitate superior resistance to corrosion, while the existence of Mn, S, and Si may form MnS and silicon oxides, which are likely to act as the initiation sites for pitting [7].

The metallographic structures of the matrix material etched in 4 g $CuSO_4$, 20 ml HCl and 20 ml ethanol, are displayed in Fig. 4. As is shown in Fig. 4(a), the material is typically austenitic in structure with the average ASTM grain size

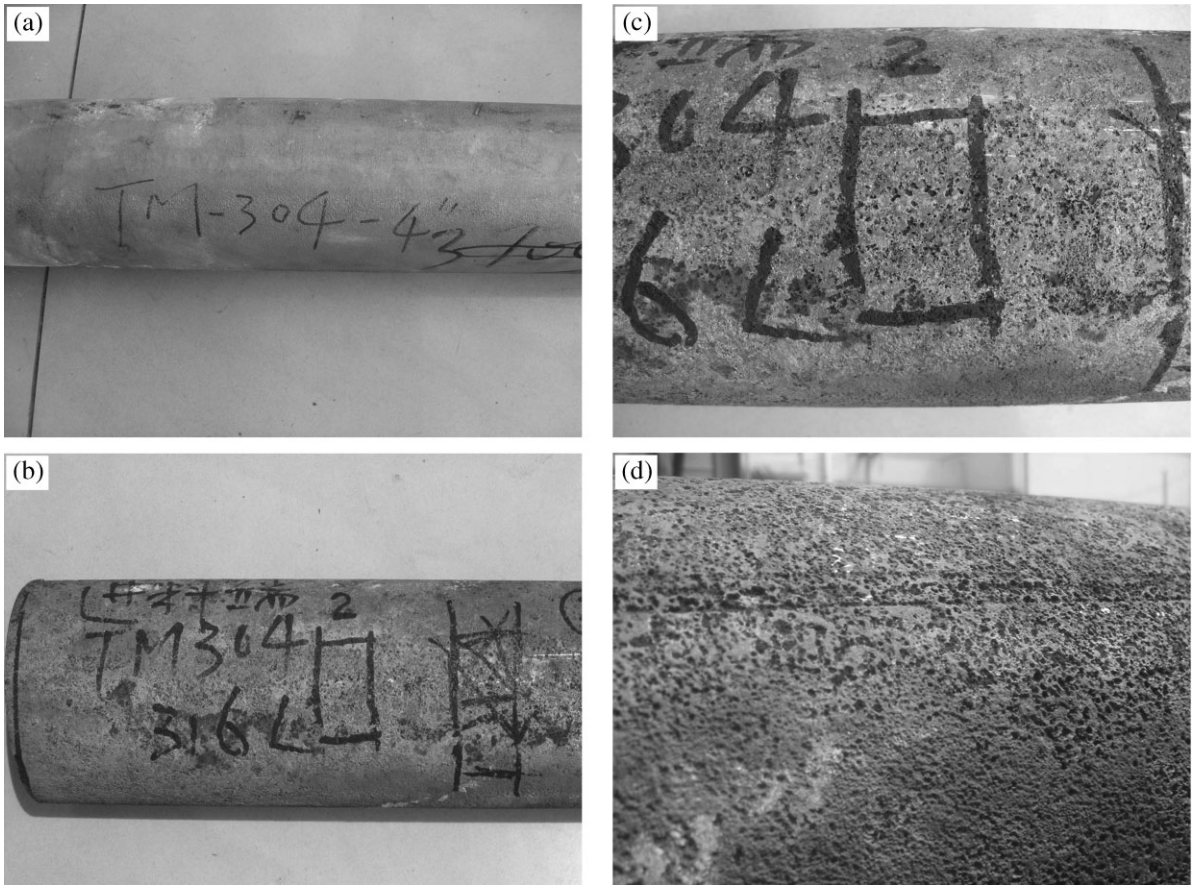

Figure 3. Macroscopic morphologies of pitted steam pipes surface; (a) pitting-free surface, (b) pitted surface, (c), (d) magnification of pitting morphology

Table 1. Chemical compositions of steam pipes (wt%)

Element	C	Si	S	P	Mn	Ni	Cr	Mo
Inlet region	0.014	0.738	0.007	0.030	1.044	12.088	17.436	2.046
Output region	0.015	0.748	0.006	0.031	1.063	12.331	17.429	2.035
SUS316L [42]	≤0.03	≤0.75	≤0.030	≤0.045	≤2.0	10.0∼14.0	16.0∼18.0	2.0∼3.0

of about 6. Also, lot of black dots, which represent the inclusions of MnS or silicon oxide, can be found within these coarse austenitic grains, as seen in Fig. 4(b). Intergranular cracks were not found in Fig. 4, which implies that stress corrosion cracking (SCC) did not occur in this case.

2.3 SEM and EDS analyses

As shown in Fig. 5(a), densely distributed corrosion pits can be seen on the pipes surface under scanning electron microscopy (SEM). In some regions, with enlargement, two neighboring pits having a diameter of about 150 μm tended to combine into a larger pit [Fig. 5(b)], which may aggravate the damage on the pipe. Figure 5(c) displays the same circumstance described in Fig. 5(b), where the number of pits is three. The white dot-like stains in Fig. 5(b) represent corrosion deposits.

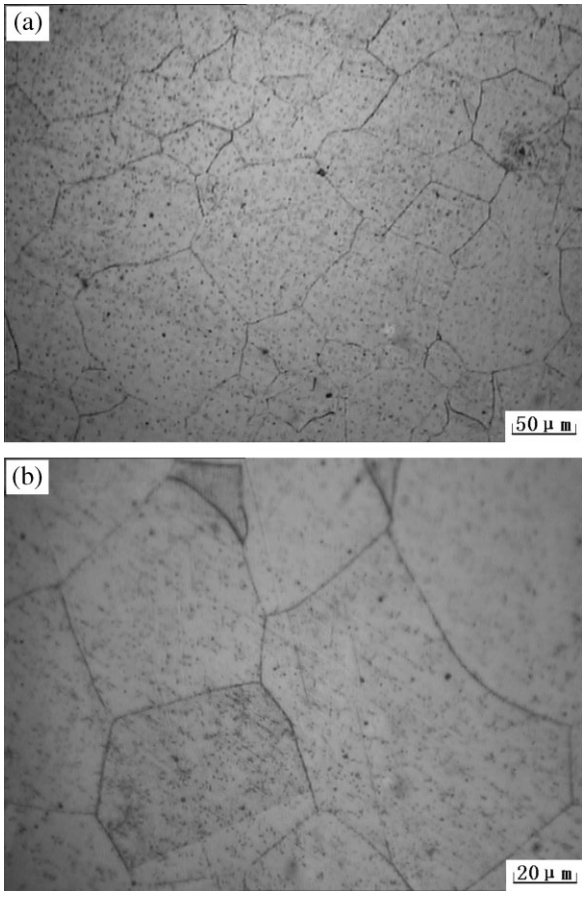

Figure 4. Metallographic structures of steam pipes with different magnifications

Samples were cut from the pitted region of the failure pipes and the cross-sections of these samples were observed under SEM. Explicit differences between the inner wall and the outer wall of the pitted pipes can be seen in Fig. 6(a) and (b). Compared

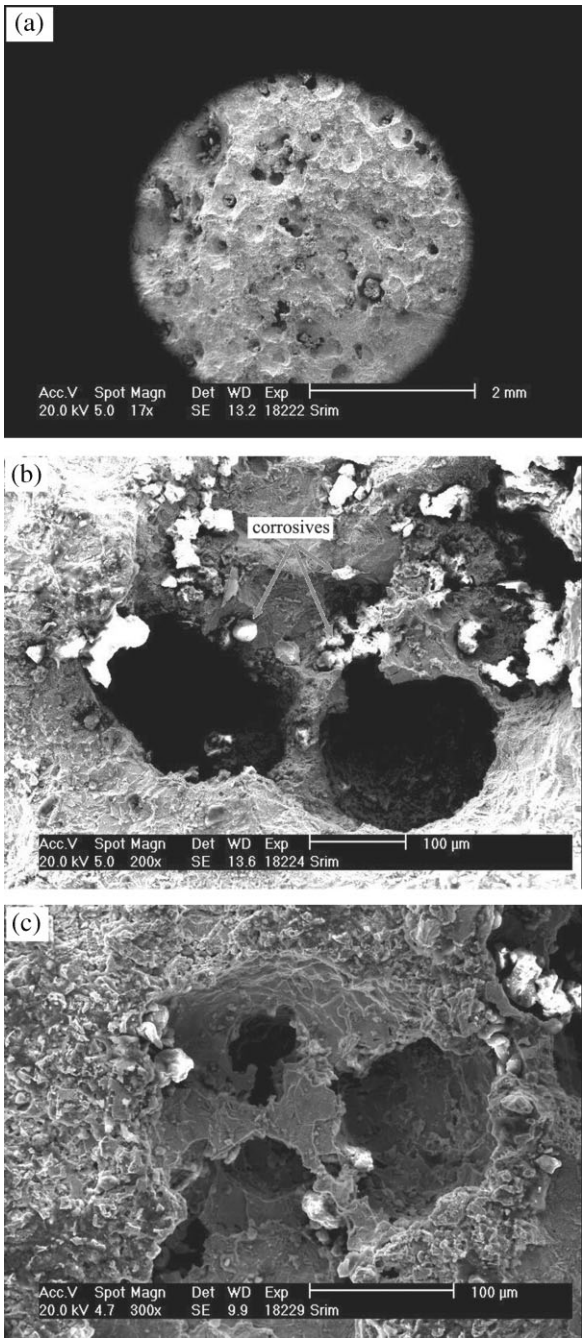

Figure 5. SEM of the pits on pipes surface; (a) total morphology, (b) two-neighboring pits, (c) three-neighboring pits

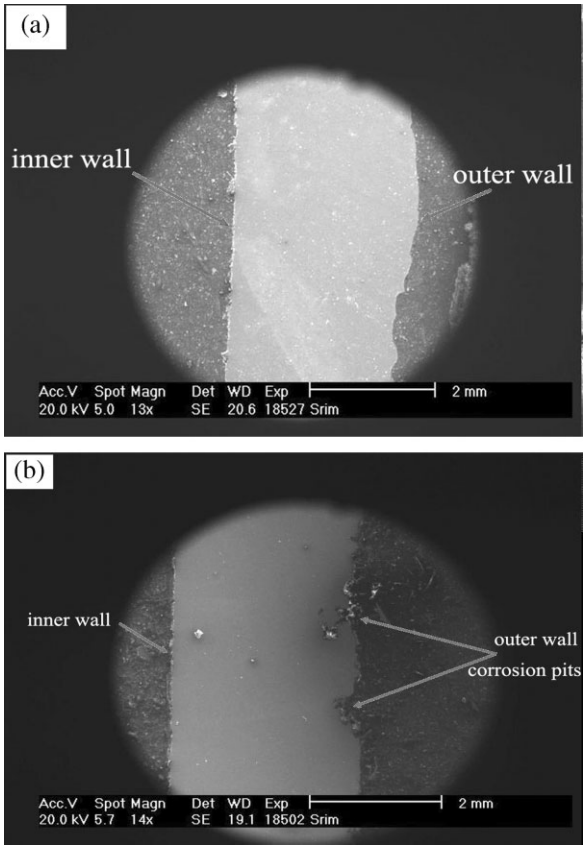

Figure 6. SEM of the cross-sections of pitted pipes

with the smooth inner wall, the outer wall was defected by some corrosion pits, whose depth had reached about 0.4 mm. As is well known, there are seven theoretical morphologies of pitting, namely, narrow and deep, elliptical, wide and shallow, subsurface, undercutting, horizontal, and vertical [8]. Schematic diagrams of the seven theoretical morphologies are displayed in Fig. 7. In this paper, it can be seen from Fig. 8 that six out of the seven theoretical pitting morphologies were obtained from the pitted pipes under SEM, which may provide a solid proof for the theoretical morphologies in practice. Indeed, the various pitting morphologies may also have caused combined side effects on the steam pipes.

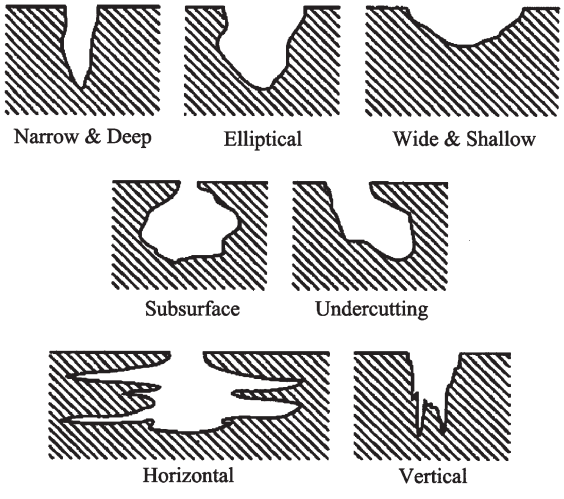

Figure 7. Schematic diagram of theoretical pitting morphologies

On taking a closer look at the corrosion deposits within the pit in Fig. 8(b), delamination can be found on the deposits, as seen in Fig. 9. It is well known that delamination may induce the deposits to be abrased layer by layer under the effect of flow (gas or liquid), which may result due to the acceleration of corrosion rate (detailed mechanisms will be discussed later). Furthermore, chemical compositions of the corrosion deposits were detected by energy dispersive spectroscopy (EDS). The four analysis sites are displayed in Fig. 9 as well, and the chemical compositions are listed in Fig. 10 and Table 2. According to the results of the analysis, it is surprising that the contents of chlorine element were 7.17, 5.36, 8.21, and 2.60% (wt%), respectively at sites A, B, C, and D. Moreover, 1.90% of the content was bromine element at site C. Hence, the EDS results verified the hypothesis proposed above that the pitting corrosion was led by the presence of halide ions.

2.4 Ion chromatography

In order to further testify the EDS results, ion chromatography (IC) was also used to identify the chemical compositions of the corrosion deposits within the pits. When dissolved in deionized water, corrosion deposits released the chloride and bromide ions they contained. Fig. 11 shows that the concentrations of the chloride and the bromide ions are 10.5 and 1.0 ppm, respectively. Although the halide ions may not induce serious corrosion with such a low content at first, they will lead the pits to grow deep inwards in the matrix material when it is accumulated in the pits. Thus, the results of ion chromatography further confirmed the causes of pitting, the halide ions.

3 Discussion

In 316L stainless steel halide ions attacking the MnS inclusions on the steam pipes' surface was the major cause of pitting. Two more reasons could be attributed for this failure: whether or not the matrix material was qualified and where the halide ions originated. Hence, research was carried out to study three aspects to identify the specific causes of pitting: the matrix materials, the process media and the service conditions. According to the analysis results, chemical compositions of the steam pipes matrix material conformed to the SUS 316L specifications, and the metallographic structure was typically austenite. Thus, it can be concluded that the matrix material was qualified; in other words, causes for the serious pitting corrosion may involve the latter two: the process media and/or the service conditions.

As was discussed above, the process media in the TA dryer consisted mainly of HAc, bromide ions, and chloride ions. Furthermore, HAc and the bromide ions were generated from the oxidation of the catalyst system, while the chloride ions were the remnants from the NaOH alkaline wash liquor. In fact, it can be inferred from the EDS and IC results for the chemical compositions of the corrosion deposits that the chloride ions were the main cause of pitting. The aggressive chloride ions commonly have two side effects on materials: SCC and pitting

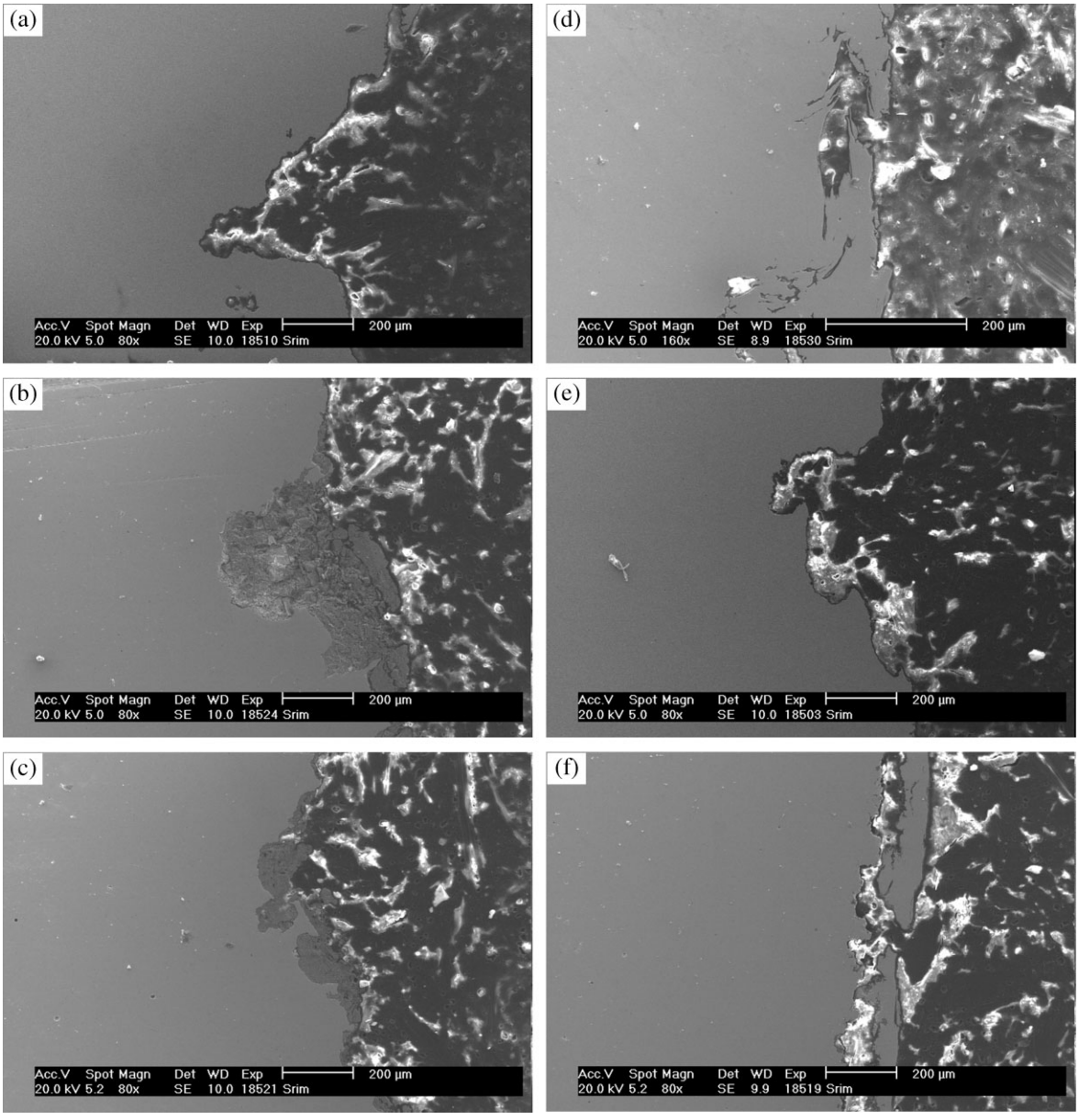

Figure 8. SEM of pitting morphologies; (a) narrow and deep, (b) elliptical, (c) wide and shallow, (d) subsurface, (e) undercutting, (f) horizontal

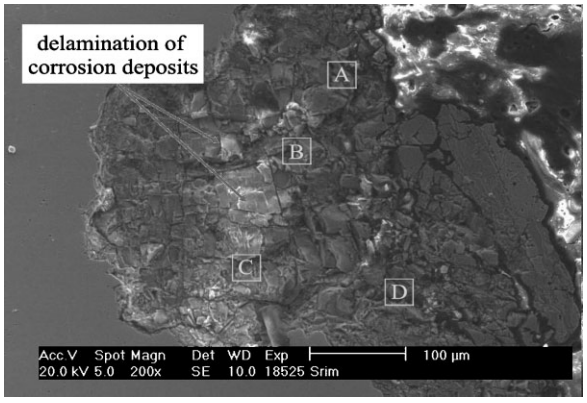

Figure 9. SEM of the delamination morphology of corrosion deposits within pit

corrosion. According to *Suresh Kumar* et al. [9], a chloride ions concentration of not less than 10 ppm is sufficient enough to cause SCC at temperatures above 60 °C. Why only pitting rather than SCC was investigated at the inlet region of the steam pipes under the environment with high chloride ions concentration at temperature above 100 °C still needs to be explained. It is well known that SCC is caused by the combined effects of three factors: tensile stress, susceptible materials, and aggressive ions, of which tensile stress is the major factor causing SCC. That the rotary steam pipes of the TA dryer are only under the compressive stress vertical to the pipes rather than the tensile stress along the pipes in service may account for why SCC did not occur in this case. Furthermore, the compressive stress was merely 0.05 kg cm^{-2} g^{-1} (about 5 kPa). So, only pitting occurred on the surface of the steam pipes.

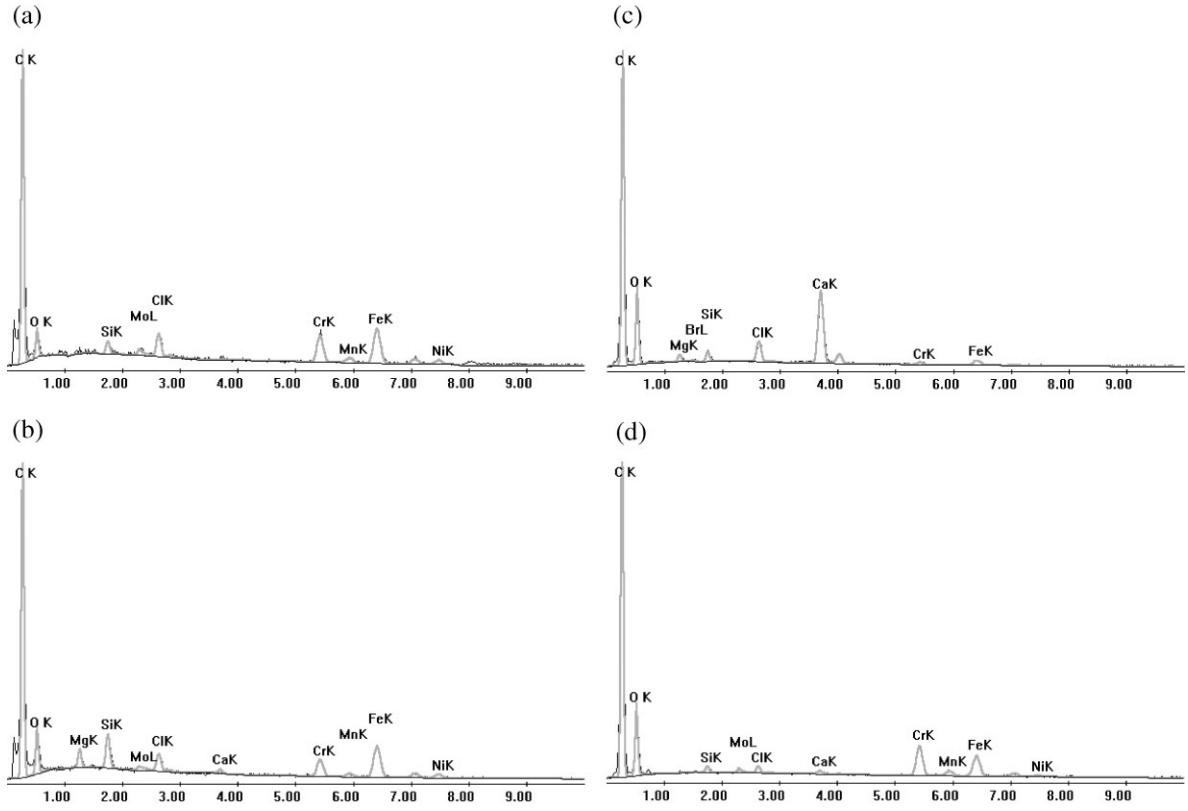

Figure 10. Chemical compositions of corrosion deposits; (a) site A, (b) site B, (c) site C, and (d) site D

Pitting is a kind of localized corrosion that selectively attacks only small areas of the metal surface but can result in relatively great damage. There is a wealth of research that had been carried out on the detailed mechanisms of pitting [10–18]. With the presence of halide ions, particularly chloride ions, susceptible sites of the passive oxide film on aluminum or stainless steel surface may be attacked by this kind of aggressive ions such as sulfide or silicon oxide inclusions [7], precipitates of carbide, defects on passive film and so on. As for stainless steel, especially those containing manganese and sulfur, MnS inclusions were always regarded as the most susceptible sites for pitting [19–29]. *Pardo* et al. [30] divided the pitting process initiated from MnS into three stages. In this paper, a different three-stage mechanism including initiation, propagation, and termination was proposed to enrich the mechanisms of pitting.

- *Initiation*

Briefly speaking, the initiation stage is a process of dissolution of MnS inclusions and formation of corrosion pits. Till date, there are two controversial theories for pit nucleation [31]: the initiation of pitting. One illustrates the competitive adsorption between Cl^- and O^{2-}, and the other describes the penetration of small-radius Cl^- into the oxide film. In detail, the former introduces a process in which the O^{2-} of the oxide film is substituted by the selectively adsorbed Cl^- and then the metal oxides are consequently converted into soluble $M^{3+}[Cl^-]_3$ complex compounds. As a result, corrosion pits are formed with the dissolution of these complex compounds. The latter theory accounts for pitting as the penetration of small-radius Cl^- into the passive film, below which the conductive ions produced by Cl^- cause the cation to move in a disorderly manner and make some specific sites of the film maintaining a high current density. If the electric field of the interface between the film and solution reaches a threshold value, pitting occurs.

Table 2. Chemical compositions of corrosion deposits (wt%)

Element	C	O	Br	Si	Mo	Cl	Cr	Mn	Fe	Ni
Site A	16.23	1.68	/*	1.68	4.33	7.17	19.44	1.76	39.02	6.44
Site B	17.15	2.95	/*	2.95	2.76	5.36	11.81	1.05	34.15	5.24
Site C	18.68	14.09	1.90	3.65	/*	8.21	2.39	/*	7.69	/*
Site D	18.83	5.51	/*	2.12	3.91	2.60	29.32	1.68	31.24	2.92

*denotes the content lower than 0.5 wt%

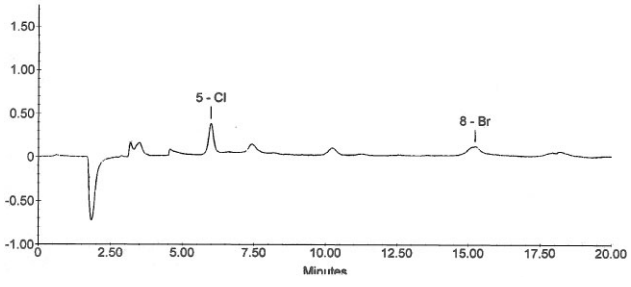

Figure 11. Ion chromatograph results of corrosion deposits within the pits

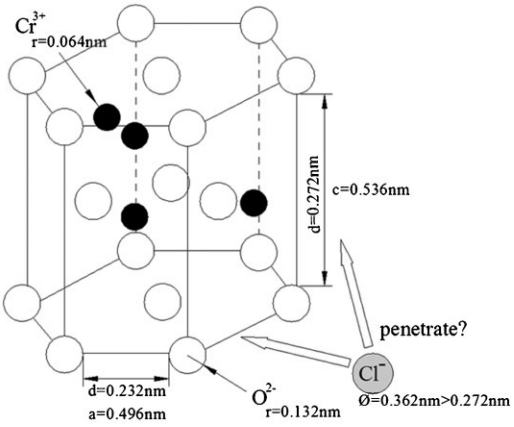

Figure 12. Schematic diagram of Cr_2O_3 crystal

As shown in Fig. 12, the Cr_2O_3 passive film of 316L represents a hexagonal closely packed (hcp) crystalline structure. Compared with the amorphous structure, the crystalline film contains a high density of imperfections such as grain boundaries, dislocations and interstices, which act as the transportion paths for small-radius ions through the passive film [32]. In a Cr_2O_3 crystal cell, oxygen ions occupy all the lattice points while the chromium ions are surrounded by six oxygen ions in the octahedral structure. It can also be derived from the literature that the lattice parameters of Cr_2O_3 hcp crystal cell are $a = 0.496$ nm and $c = 0.536$ nm [33]. As the radii of oxygen and chromium ions are 0.132 and 0.064 nm [34], respectively, the actual distances between two lattice points are 0.232 and 0.272 nm, respectively, corresponding to the lattice parameters a and c. Therefore, it is noted that the lattice interstices are not wide enough for a chloride ion with radius of 0.181 nm, i.e. the diameter is 0.362 nm, to penetrate. Thus, it is obvious that the latter theory that ascribes the transport of chloride ions through the Cr_2O_3 passive film for pitting initiation may not be true.

In this paper, a novel mechanism, different from the two theories mentioned above, is put forward. Actually, it can be learned from Fig. 4 that the MnS inclusions are not completely beneath the Cr_2O_3 film. Hence, emphasis should be laid on the direct attack of chloride ions on the MnS inclusions. Sulfur and chlorine being two neighboring elements in the Periodic Table of Elements, their ions possess similar radii, which are 0.174 and 0.181 nm, respectively [34]. Due to the very small difference between the radii of the two ions, the sulfide ions in thermodynamically unstable MnS inclusions may be substituted by the chloride ions. As a result, soluble $Mn^{2+}[Cl^-]_2$ complex compounds are produced. Finally, $M^{3+}[Cl^-]_3$ dissolves and leads to the formation of Mn^{2+} ions [equation (3)] and the corrosion pits (Fig. 13).

$$MnS \xrightarrow{HAc/Cl^-} Mn^{2+} + S + 2e^- \quad (3)$$

- *Propagation*

The propagation stage involves the generation and accumulation of hydrogen ions within the corrosion pits as well as the

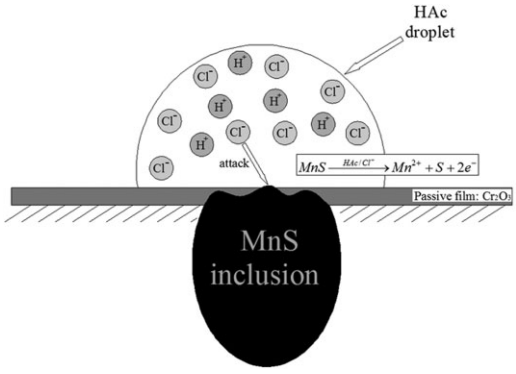

Figure 13. Schematic diagram of the initiation stage of pitting

accelerated inward growth of pits in the matrix. On the one hand, hydrolysis reaction [equation (4)] of the metal cations that were generated in the initiation stage favors a local increase of hydrogen ion concentration, which may introduce an exceedingly low pH environment in the pits' interior with the association of the hydrogen ions originating from HAc [equation (5)]. Furthermore, in order to keep electrical neutrality, the chloride ions migrate inwards in the pits while the ferrous ions (II) in the pits migrate outwards (Fig. 14). Thus, the aggressive medium in the corrosion pits is actually the hydrochloric acid (HCl), which will increase the growth rate of pitting. On the other hand, oxidative metal cationic ions such as Fe^{3+} and Mo^{2+} may also accelerate the growth of pitting due to its high reduction potential in association with chloride ions, i.e. the depolarization effect [35]

$$M^{n+} + nH_2O \rightarrow M(OH)_n + nH^+ \quad (4)$$

$$HAc \rightleftarrows H^+ + Ac^- \quad (5)$$

In fact, the propagation stage is an autocatalytic process assisted by the occluded corrosion cell (OCC). It can be learned from Fig. 14 that, with the outward migration of ferrous ions (II), ferric hydroxide [$Fe(OH)_3$] is formed and gets deposited at the pits' mouth [equation (7)], which results in an occluded area in the pits interior [36]. The matrix material exposed to HCl within

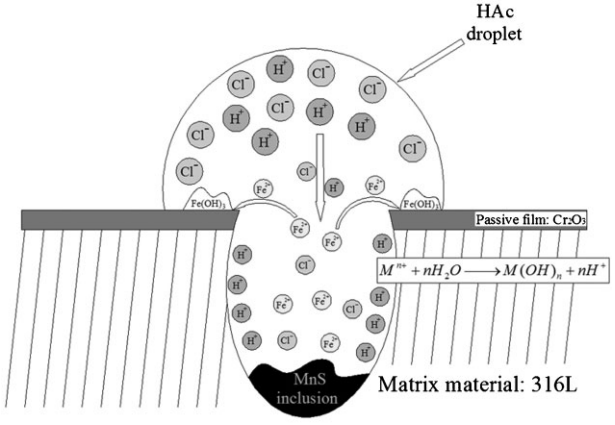

Figure 14. Schematic diagram of the propagation stage of pitting

the pits serves as the anode due to its activated status, while the Cr_2O_3 passive film outside the pits acts as the cathode. Such a 'small anode–large cathode' OCC will spontaneously cause the pits to grow inwards in the matrix in a deep and narrow form. Thus, the hydrogen ions in the pits' interior continuously attack the matrix to produce metal cations, which hydrolyze to generate hydrogen ions in turn, i.e. the autocatalytic process.

$$Fe^{2+} + 2OH^- \rightarrow Fe(OH)_2 \quad (6)$$

$$Fe(OH)_2 + 2H_2O + O_2 \rightarrow 4Fe(OH)_3 \downarrow \quad (7)$$

- *Termination*

The termination stage can also be defined as the repassivation of the matrix metal in the corrosion pits. According to *Pardo* et al. [30], highly stable and insoluble compounds like $FeMnO_4$ and MoO_3 form and cover the wall of the corrosion pits under the condition of low pH and high potential values. As a result, the potential values within the pits will then transfer to the passivation region; in other words, the repassivation begins and the pitting growth terminates.

Regarding the corrosion rate of 316L steel in the acetate acid containing halide ions, some experiments on the corrosion depth were carried out [37, 38]. *Mattsson* [39] defined the corrosion rate of qualified stainless steel to be not more than 0.1 mmy^{-1}. Fig. 6(a) provides the evidence of thinning of the pitted pipes, for a thickness of 2.74 mm compared with its original value of 3.0 mm. Service conditions of the steam pipes may be attributed cause for such a serious thinning. As shown in Fig. 2, the steam pipes in the inlet region of TA dryer contact both the wet TA cakes and the carrier gas, which may lead to a two-phase (gas and liquid) FAC on the steam pipes' surface due to the high humidity of the wet TA cakes [40, 41]. FAC is a kind of corrosion process of chemical dissolution of metal that always leads to thinning of pipes. That the corrosion deposits produced by aggressive liquid on the surface will be removed layer by layer by high-flow-rate gas may account for the acceleration effect from FAC. In this case, the metastable pipes' surface with delaminated corrosion deposits within the pits (Fig. 9) was abrased by carrier gas and it eventually resulted in thinning of its wall thickness. Thus, the cause for the serious pitting corrosion taking place only at the inlet region rather than at other parts of the steam pipes can be explained. The relatively high temperature near 130 °C is also a critical factor inducing the acceleration effect. According to *Hou Feng*'s [37] experiments, the corrosion rate of 316L steel under the environment stimulated from the actual service condition of TA dryer (26.2% TA, 0.96% Br^-, 67.11% HAc (wt%) at 110 °C) reached even 1 mmy^{-1}. Finally it can be concluded that the serious corrosion situation and a quite high corrosion rate on the inlet region of steam pipes resulted from the interaction between pitting, FAC, and high temperature.

4 Conclusions

1. Chloride ions from the NaOH alkaline wash liquor were the primary factor for the occurrence of pitting which took place on the steam pipes' surface with matrix material of standard 316L austenitic stainless steel in TA dryer.
2. The harsh environment, i.e. the high temperature of about 130 °C and the FAC effect around the inlet region of TA dryer were the main factors for the acceleration of pitting corrosion.
3. The small-radius chloride ions (0.181 nm) substituting for the sulfide ions (0.174 nm) of MnS inclusions and forming the soluble $Mn^{2+}[Cl^-]_2$ complex compounds may favor the initiation of pitting.
4. Six types of pitting morphologies were obtained in engineering practice to prove and enrich all the seven theoretical morphologies.
5. Several countermeasures such as limiting the chloride ion concentration in the alkaline wash liquor under 30 ppm and good control of the service temperature in TA dryer were implemented to mitigate the extent of pitting.

Acknowledgements: This work was supported by both Shanghai Petrochemical Co., Ltd. and Shanghai Leading Academic Discipline Project (Project no. B113).

5 References

[1] H. Macarie, A. Noyola, J. P. Guyot, *Water Sci. Technol.* **1992**, *25*, 223.
[2] Y.-H. Liu, R.-G. Chen, Q. Zheng, *Chem. Eng. Des.* **2000**, *10*, 29 (in Chinese).
[3] N. Pernicone, M. Cerboni, G. Prelazzi, F. Pinna, G. Fagherazzi, *Catal. Today* **1998**, *44*, 129–135.
[4] G. R. Pophali, R. Khan, R. S. Dhodapkar, T. Nandy, S. Devotta, *J. Environ. Manage.* **2007**, *85*, 1024.
[5] M. H. Moayed, M. Golestanipour, *Mater. Corros.* **2005**, *56*, 39.
[6] B. R. Tzaneva, L. B. Fachikov, R. G. Raicheff, *Corros. Eng. Sci. Technol.* **2006**, *41*, 62.
[7] P. Poyet, P. Couchinave, J. Hahn, B. Saulnier, J. Y. Boos, *Mem. Sci. Rev. Met.* **1975**, *72*, 133.
[8] *ASTM G46-94-1999*, Standard Guide for Examination and Evaluation of Pitting Corrosion.
[9] M. Suresh Kumar, M. Sujata, M. A. Venkataswamy, S. K. Bhaumik, *Eng. Fail. Anal.* **2008**, *15*, 497.
[10] T. J. Hakkarainen, *Mater. Corros.* **2003**, *54*, 503.
[11] A. Pardo, E. Otero, M. C. Merino, *Mater. Corros.* **2000**, *51*, 850.
[12] G. T. Burstein, C. Liu, R. M. Souto, S. P. Vines, *Corros. Eng. Sci. Technol.* **2004**, *39*, 25.
[13] X. Shi, R. Avci, M. Geiser, *Corros. Sci.* **2003**, *45*, 2577.
[14] J. K. Glenn, M. H. Gold, *Arch. Biochem. Biophys.* **1985**, *242*, 329.
[15] C. R. McCall, M. A. Hill, R. S. Lillard, *Corros. Eng. Sci. Technol.* **2005**, *40*, 337.
[16] B. J. Little, P. A. Wagner, Z. Lewandowski, presented at *Proc. Corrosion '99*, NACE, Houston, USA, **1999**, pp. 294.
[17] P. Ernst, R. C. Newman, *Corros. Sci.* **2002**, *44*, 927.
[18] P. Ernst, R. C. Newman, *Corros. Sci.* **2002**, *44*, 943.
[19] B. Vuillemin, X. Philippe, R. Oltra, V. Vignal, L. Coudreuse, L. C. Dufour, E. Finot, *Corros. Sci.* **2003**, *45*, 1143.
[20] J. S. Noh, N. J. Laycock, W. Gao, B. Wells, *Corros. Sci.* **2000**, *42*, 2069.
[21] A. Rossi, R. Tulifero, B. Elsener, *Mater. Corros.* **2001**, *52*, 175.

[22] G. S. Eklund, *J. Electrochem. Soc.* **1974**, *121*, 467.
[23] A. Szummer, Z. Szklarska-Smialowska, M. Janik-Czachor, *Corros. Sci.* **1968**, *8*, 833.
[24] M. Smialowskiy, Z. Szklarska-Smialowska, M. Rychick, A. Szummer, *Corros. Sci.* **1969**, *9*, 123.
[25] Z. Szklarska-Smialowska, A. Szummer, M. Janik-Czachor, *Br. Corros. J.* **1970**, *5*, 159.
[26] E. Lunarska, Z. Szklarska-Smialowska, M. Janik-Czachor, *Corrosion* **1975**, *31*, 231.
[27] J. Crolet, L. Seraphin, R. Tricot, *Mem. Sci. Rev. Met.* **1977**, *74*, 647.
[28] J. Stewart, D. E. Williams, *Corros. Sci.* **1992**, *33*, 457.
[29] M. A. Baker, J. E. Castle, *Corros. Sci.* **1993**, *34*, 667.
[30] A. Pardo, M. C. Merino, A. E. Coy, F. Viejo, R. Arrabal, E. Matykina, *Corros. Sci.* **2008**, *50*, 1796.
[31] Yue Sun, Jin Hu, *Corrosion and Control of Metals*, Harbin Industry University Press, Harbin, China **2003**, (in Chinese).
[32] D. H. Hur, Y. S. Park, *Corrosion*, **2006**, *62*, 745.
[33] Yang. Li-jun, *J. West. Chongqing Univ.* (Nat. Sci. Edn.) **2003**, *2*, 9 (in Chinese).
[34] J. P. Schaffer, A. Saxena, S. D. Antolovichm et al. *The Science and Design of Engineering Materials*, 2nd edn., McGraw-Hill, New York **1999.**
[35] P. Sędek, J. Brózda, J. Gazdowicz, *Eng. Fail. Anal.* **2008**, *15*, 281.
[36] K. R. Trethewey, J. Chamberlain, *Corrosion for Science and Engineering*, 2nd edn., Longman, Essex **1998.**
[37] Hou. Feng, Xu. Hong, Xu. Linyun et al., *China Syn. Fiber Ind.* **2005**, *28*, 34 (in Chinese).
[38] A. Turnbull, M. Ryan, A. Willetts, S. Zhou, *Corros. Sci.* **2003**, *45*, 1051.
[39] E. Mattsson, *Basic Corrosion Technology for Scientists and Engineers*, Ellis Horwood Limited, West Sussex **1989.**
[40] C. Hales, K. J. Stevens, P. L. Daniel, M. Zamanzadeh, A. D. Owens, *Eng. Fail. Anal.* **2002**, *9*, 235.
[41] R. B. Dooley, V. K. Chexal, *Int. J. Pres. Ves. Pip.* **2000**, *77*, 85.
[42] *ASME N-708-2007*, Use of JIS G4303, Grades SUS304, SUS304L, SUS316, and SUS316L Section III, Division 1, SUPP 2.

(Received: November 20, 2008)
(Accepted: December 10, 2008)
W5198

